Published in *Materials Science and Engineering A*, 655, 2016, pp60-69. Doi: 10.1016/j.msea.2015.12.086

# Achieving superior grain refinement and mechanical properties in vanadium through high-pressure torsion and subsequent short-term annealing

Yi Huang[a, *], Mathilde Lemang[b], Nian Xian Zhang[a],
Pedro Henrique R. Pereira[a], Terence G. Langdon[a]

[a]Materials Research Group, Faculty of Engineering and the Environment,
University of Southampton, Southampton SO17 1BJ, U.K.
[b]Phelma - School of Engineering in Physics, Electronics and Materials,
Grenoble INP Minatec, 3 Parvis Louis Neel, BP 257, 38016 Grenoble Cedex 1, France.

[*] Corresponding author: Yi Huang; e-mail: y.huang@soton.ac.uk

**Abstract**

Commercial purity vanadium with an initial grain size of ~27 μm and a Vickers microhardness of Hv ≈ 85 was processed by high-pressure torsion (HPT) under a pressure of 6.0 GPa at room temperature through 1/2 to 10 turns. After processing through 10 turns, some samples were immediately subjected to a short-term annealing (15 min) at different temperatures from 773 to 1173 K. The microstructures developed in HPT and in HPT plus post-HPT annealing were characterized by electron backscatter diffraction (EBSD). Processing by HPT for 10 turns gave a refined grain size of ~410 nm and an increased hardness of Hv ≈ 240. Post-HPT annealing demonstrated that the ultrafine grained vanadium has good thermal stability up to at least 873 K. Tensile testing at room temperature gave an ultimate tensile strength of ~920 MPa after 10 turns of HPT with an elongation of ~29%. These results show HPT processing produces superior mechanical properties in vanadium by comparison with processing by ECAP or ECAP plus cryorolling.

**Keywords**: hardness, high-pressure torsion, short-term annealing, ultrafine-grained materials, vanadium.

## 1. Introduction

Vanadium is a refractory metal having a body-centred cubic (bcc) structure with a high melting temperature (2163 K). It is soft and ductile and has good forming properties at low temperatures [1]. It also has a high strength at high temperatures with a brittle-to-ductile transition temperature which is low compared with other refractory metals [2]. Vanadium is used mostly in industry as an additive to steels or titanium alloys in order to increase the strength, hardness and high temperature stability.

Vanadium has received considerable attention in nuclear applications because it has the lowest capture cross-section for high energy neutrons of all refractory metals (~1.5 m barns for 1 MeV neutrons) combined with good structural strength and a high melting point [3]. Thus, vanadium is a leading candidate material for first-wall and blanket structures in fusion reactors [4-8]. It is well known that vanadium is chemically reactive with gaseous interstitial impurities, such as oxygen and nitrogen, and this would produce interstitial embrittlement with an increase in yield strength and hardness and an accompanying loss in ductility and formability [7,9-10].

In practice, interstitial embrittlement is a major deterrent for using vanadium in nuclear reactor applications and it is generally attributed to an overall weakness of the grain boundary bonding strength [11]. Furthermore, it is anticipated that irradiation by fast neutrons, at temperatures between ~$0.3 - 0.5T_m$ where $T_m$ is the absolute melting temperature, may also produce swelling by void formation and growth processes depending upon the fluence, temperature, gas content and microstructure. It is generally recognized that a refinement of the grain size will reduce the irradiation-produced vacancy supersaturation which is required for void nucleation and growth [3]. Thus, it is reasonable to anticipate that the development of vanadium with an ultrafine grain size will be beneficial in reducing the

interstitial embrittlement and swelling during radiation and thereby it will significantly enhance the potential for nuclear applications.

Attempts were reported for achieving a fine-grained structure in Y-containing vanadium alloys through mechanical alloying and hot isostatic pressing (HIP) followed by annealing [8-10] and in pure vanadium via HIP and annealing [12]. However, it is recognised that these powder metallurgy products may suffer from contamination and residual porosity which would hinder their application in nuclear reactors.

It is well known that significant grain refinement may be introduced in bulk polycrystalline materials through the application of severe plastic deformation (SPD) [13-15], with the processed grain sizes typically lying within the submicrometer or even the nanometer range. Among various SPD techniques, the most common procedures are equal-channel angular pressing (ECAP) [16] and high-pressure torsion (HPT) [17] where ECAP requires repetitive pressings in order to achieve large strains whereas HPT leads to exceptionally high strains in a single processing operation. In practice, HPT is especially attractive because, by comparison with ECAP, it produces both smaller grains [18, 19] and a higher fraction of grain boundaries having high angles of misorientation [20].

To date, there are only a limited number of reports describing the processing of vanadium to produce microstructural refinement using SPD techniques [11,21-24]. Earlier experiments showed that the grain refinement in vanadium saturated after eight passes of ECAP processing [21] and therefore cryogenic rolling was introduced after ECAP in order to achieve additional refinement by imposing a further 60% strain by cryorolling [11,22]. These materials showed increases in the ultimate tensile strength (UTS) from ~750 MPa after ECAP to ~920 MPa after ECAP plus cryorolling but this was accompanied by a ductility loss so that the total elongations to failure for these two processing routes were reduced from ~14% to ~8.5% [11]. Very recently there have been two reports describing grain refinement of pure

vanadium processed by HPT [23,24] and these results show that the material exhibits little or no ductility.

Considering the limited ductility attained in the ECAP plus cryorolled condition and the lack of any systematic evaluation of microstructural evolution during HPT processing, the present research was initiated to study the modifications that may be introduced in pure vanadium by combining HPT processing and subsequent short-term annealing. The overall objective of this research was to establish a material processing procedure that may be used to refine the microstructure and enhance the properties in order to achieve a high strength vanadium with improved ductility

## 2. Experimental material and procedures

Vanadium of 99.8% purity was supplied by Goodfellow Ltd (Cambridge, UK) with typical trace elements (in ppm) of Ag 1, Al 2, Ca <1, Cr 15, Cu <1, Fe 70, Mg <1, Mn 1, Si 300. The as-received vanadium was in a rolled state in the form of rods having diameters of 11 mm. These as-received rods were annealed at 1173 K for 1 h in a vacuum furnace and this is henceforth designated the as-annealed state. The rod was then machined to a diameter of 9.9 mm, sliced into discs with thicknesses of ~1.2 mm and these discs were ground with abrasive papers to final thicknesses of ~0.8 mm.

All discs were processed by HPT at room temperature through total numbers of turns, *N*, of 1/2, 1, 5 and 10 using an imposed pressure of 6.0 GPa and a rotational speed for the lower anvil of 1 rpm. The HPT was conducted under quasi-constrained conditions where there is a small outflow of material around the periphery of the disc during the processing operation [25,26],

To investigate the thermo-stability of the HPT-processed discs, samples processed through 10 turns were removed from the HPT facility and then immediately annealed for short times of 15 min at temperatures of 773, 873, 973, 1073 or 1173 K. These annealing

temperatures were selected based on an earlier report presenting microstructural analysis as a function of annealing temperature for vanadium processed by ECAP where recrystallization was almost complete at 973 K after annealing for 1 h [21]. Considering the small size of the HPT discs, and in order to avoid recrystallization which may cause strength loss and grain growth, the HPT-processed samples were subjected to only very short-term anneals of 15 min. This is henceforth designated the post-HPT annealed condition.

For microstructural analysis, discs were examined in the as-annealed condition, in the HPT-processed condition and in the post-HPT annealed condition. These discs were hot-mounted in bakelite, ground with abrasive papers and then a final polish was performed using a colloidal silica solution in order to produce a mirror-like surface. For the as-annealed sample, the polished surface was etched using a solution of 30 mL of 32% hydrochloric acid (HCl), 15 mL of 65% nitric acid ($HNO_3$) and 30 mL of hydrofluoric acid (HF) with an etching time of 10 to 20 s. The sample surface was then observed in dark field using an Olympus BX51 optical microscope in order to determine the initial grain structure. The average grain size was measured by the linear intercept method using Image J software and measurements of more than 300 grains. The grain structures after HPT processing and post-HPT annealing were examined by electron backscattered diffraction (EBSD) using a JSM6500F thermal field emission scanning electron microscope (SEM). The EBSD patterns were collected using a step size of 60 nm and a cleaning procedure was applied such that the total numbers of modified points were less than 10% of all points measured. High-angle grain boundaries (HAGBs) were defined as boundaries having misorientation differences between adjacent measuring points of more than 15° and low-angle grain boundaries (LAGBs) had misorientation differences of 2° – 15°.

Hardness measurements were taken using an FM300 hardness tester equipped with a Vickers indenter with a load of 300 gf and a dwell time of 15 s. The hardness values on the

HPT-processed samples were measured after $N$ = 0.5, 1, 5 and 10 turns by mapping the values of Hv over the total surface of each disc. Specifically, the individual values of Hv were recorded following a rectilinear grid pattern with a separation of 0.3 mm between each adjacent point [27]. All of these values were then used to construct colour-coded contour maps that provided a clear visual presentation of the distributions in hardness across the surface of each disc. The hardness values on the as-annealed and post-HPT annealed samples were measured along disc diameters with a separation distance of 0.3 mm between neighbour points.

Tensile tests were conducted using the as-annealed sample, the HPT-processed samples and the post-HPT annealed samples. Following earlier practice [28], and in order to avoid any microstructural inhomogeneities in the centres of the discs, two tensile specimens were prepared from each disc using electro-discharge machining and with the specimens arranged symmetrically on either side of the disc centre. These miniature tensile specimens had gauge lengths and widths of 1 mm. The tensile specimens were pulled to failure at room temperature using a Zwick 30 KN Proline testing machine operating at a constant rate of cross-head displacement with an initial strain rate of $1.5 \times 10^{-3}$ $s^{-1}$.

## 3. Experimental results

### *3.1 Microstructure evolution during HPT processing*

In the initial as-annealed condition, the vanadium had a uniform equiaxed microstructure with an average grain size of ~27 μm and an average hardness of Hv ≈ 85.

The microstructural development after HPT processing is shown in Fig. 1 with the centre areas of the discs on the left, the edge areas on the right and images displayed in the order of 1/2, 1, 5 and 10 turns, respectively: the colours denote different grain misorientations as depicted in the unit triangle on the right, LAGBs (2°-15°) are shown in yellow and HAGBs (>15°) in black. After 1/2 turn the microstructures are markedly inhomogeneous in the centre

and edge areas, the microstructure is coarse in the centre area but there is significant grain refinement at the edge with an average grain size of ~350 nm. After 1 turn the microstructures are more homogeneous with average grain sizes of ~345 and ~320 nm in the centre and edge areas, respectively. After 5 turns, the grain sizes increase slightly to ~415 and ~350 nm at the centre and edge and after 10 turns the microstructures are essentially uniform with similar average grain sizes of ~405 and ~410 nm at the centre and edge, respectively. There is some evidence after 10 turns for the appearance of a very small number of slightly larger grains in both the centre and edge regions and this suggest the onset of structural recovery in both regions.

In order to clearly display the effect of the numbers of HPT turns on the evolution of the grain misorientation distributions, these data are shown in Fig. 2 for different numbers of turns in (a) the centre region and (b) the edge region, respectively: these misorientation distributions correspond to the conventional pixel-to-pixel distributions recorded by orientation imaging and it is recognized that this may not correspond precisely to the grain-to-grain misorientation distributions because it often leads, as in Fig. 2(a), to a large fraction of LAGBs [29].

Inspection of Fig. 2 shows that the misorientation distributions in the centres of the discs are significantly different between 1/2 turn and all other conditions. At 1/2 turn there is a high fraction of LAGBs (~84.6%) but this fraction decreases to only ~21.1% after 1 turn. A detailed summary of the measured fractions of LAGBs and HAGBs is given in Table 1 for each processing condition shown in Fig. 2. For the centre position it is readily apparent that the grain structure gradually evolves from a coarse structure to a fine structure with additional numbers of turns whereas at the edge of the disc there are almost no changes in the misorientation distributions with increasing torsional straining and the fraction of HAGBs is

very high at ~87.4% even after 1/2 turn. These measurements demonstrate that grain refinement at the edge of the disc proceeds very rapidly in the earliest stages of HPT.

*3.2 Hardness evolution during HPT processing*

Hardness mapping provides a simple visualisation of the hardness evolution and distribution throughout the surfaces of the discs after HPT processing through different numbers of turns. The hardness values for four discs are displayed pictorially as colour-coded contour maps in Fig. 3 where the upper row is for 1/2 and 1 turn, the lower row is for 5 and 10 turns and the individual values of Hv are represented by a set of unique colours denoting values from 100 to 300 in incremental steps of 50 as shown by the colour key on the right. In these plots, the coordinate system *X* and *Y* denotes two randomly selected perpendicular axes that are superimposed on the discs such that the central point in every disc is given by the coordinates (0, 0).

The results in Fig. 3 show the evolution of hardness from a markedly non-uniform distribution after 1/2 turn to a uniform distribution after 10 turns. Inspection shows there is a large area of lower hardness after 1/2 turn but this area shrinks towards the disc centre after 1 turn, contracts further after 5 turns and essentially disappears after 10 turns. A direct comparison of the contour maps after 5 and 10 turns shows that these maps exhibit slightly different colours which signify a very small hardness drop between 5 and 10 turns. This drop suggests the onset of some limited recovery during HPT processing. It is important to note that all colour-coded maps are symmetrical around their central points.

*3.3 Microstructure and hardness evolution during post-HPT annealing*

In order to investigate the effect of a post-HPT annealing on microstructure and hardness development, samples were processed by HPT through 10 turns and then annealed for 15 min at temperatures from 773 to 1173 K. Figure 4 shows representative microstructures developed after short-term annealing at (a) 773, (b) 873, (c) 973 and (d) 1073

K, respectively: it is important to note that Figs 4(a), (b) and (c) have the same magnification but Fig. 4(d) has a lower magnification.

The microstructure after short-term annealing at 773 K looks very similar to the initial microstructure at the edge of the sample shown in Fig. 1(h) after 10 turns. Furthermore, the measured grain size was ~410 nm which is the same as after 10 turns of HPT. After annealing at 873 K in Fig. 4(b), some coarser grains are visible but overall the structure remains essentially unchanged with an average grain size of ~420 nm. Increasing the annealing temperatures to 973 K leads to very clear grain growth as in Fig. 4(c) where the average grain size increases to ~760 nm. This larger grain size confirms the advent of recrystallization when annealing at 973 K and this is consistent with earlier results [21]. Finally, annealing at 1073 K leads to very significant grain growth as shown in Fig. 4(d) where the average grain size increases to ~2.84 μm.

The overall microhardness values and the variations in grain size after post-HPT annealing are plotted in Fig. 5. It is apparent that the microhardness values show a sigmoidal relationship with the annealing temperature where the values are essentially on a plateau from room temperature (296 K) to ~773 K, they drop sharply from ~773 to ~1073 K and at even higher temperatures there is again a reasonable plateau. The sharp drop at intermediate annealing temperatures is associated with the microstructural changes and the consequent grain growth with increasing annealing temperature as documented in Fig. 4.

*3.4 Tensile properties of HPT-processed and post-HPT annealed samples*

By considering the hardness and grain size variations during post-HPT annealing as documented in Fig. 5, three samples were selected for tensile testing after short-term anneals at 773, 873 and 973 K. The result is shown in Fig. 6 where stress-strain curves obtained at room temperature with an initial strain rate of $1.5 \times 10^{-3}$ $s^{-1}$ are plotted for the three post-HPT annealed samples plus an as-annealed sample and a sample processed by HPT for 10 turns.

Inspection shows that the as-annealed material has a low UTS of ~260 MPa and a relatively large elongation of ~79% whereas after HPT processing to 10 turns the strength is increased to ~920 MPa but the elongation is reduced to only ~29%.

The effects of post-HPT annealing are visible in Fig. 6. Annealing at 773 K has only a minor effect of the UTS and elongation but annealing at 873 K reduces the UTS to ~750 MPa and increases the elongation to ~39%. A further increase in annealing temperature to 973 K reduces the UTS to ~420 MPa but further increases the elongation to ~50%. All values for the UTS and elongations are summarized in Table 2 and it is apparent that an increase in the short-term annealing temperature leads to a lower material strength but an improved ductility.

It is interesting to note that Fig. 6 also shows yield drops for samples processed with post-HPT annealing at 873 and 973 K and this drop is most significant after annealing at 873 K. By contrast, the sample subjected to a post-HPT annealing at 773 K shows a normal smooth yielding.

*3.5 Texture development during HPT processing and post-HPT annealing*

Inverse pole figures are shown in Fig. 7 for the disc centres and edges after 1/2 and 10 turns of HPT processing where $Z_0$ denotes the axis direction perpendicular to the disc surface. After 1/2 turn, the disc centre has coarse grains but the disc edge exhibits significant grain refinement as shown in Fig. 1(a) and (b), respectively. The inverse pole figures for these samples are given in Fig. 7(a) and (b) where a {212} texture develops on the disc surface in the centre area but a {110} texture develops at the edge. After 10 turns, as in Fig. 7(c) and (d), both centre and edge show similar {110} textures. Generally in bcc crystals slip occurs in the close-packed <111> direction and the Burgers vector is $a/2$ <111> where $a$ is the lattice parameter. The planes with the largest interplanar spacings are {110} followed by {112} and then {123}. In practice, during HPT processing the torsion strain is applied in a direction

parallel to the disc surface so that the development of a {110} texture during HPT confirms the occurrence of slip on the {110} plane to accommodate the severe torsional strain.

An examination of microstructure development during post-HPT annealing in Fig. 4 shows that many grains having similar orientations appear in the microstructure as the short-term annealing temperature is increased to 973 and 1073 K and these grains have their {110} planes parallel to the disc surface as indicated in the unit triangle in Fig. 1. Figure 8 shows the inverse pole figures from microstructures after post-HPT annealing at 873, 973 and 1073 K where $Z_0$ again represents the axis direction perpendicular to the disc surface. At 973 K the material has a slightly stronger {110} texture than at 873 K because there is a slightly higher texture intensity maximum value at 973 K. By contrast, there is a fully-recrystallized microstructure at 1073 K and a strong and sharp {110} texture develops on the disc surface.

An earlier report described fiber texture development in ECAP-processed vanadium with post-ECAP annealing [21]. The main features of the texture characteristics of as-ECAP samples remained unaltered by the post-ECAP annealing but the intensity of the orientation components increased with annealing temperature. There is a similar texture development in the HPT-processed vanadium subjected to subsequent short-term annealing. Thus, during post-HPT annealing at 873 and 973 K the hardness is continuously reduced, the material experiences recovery and partial recrystallization so that the texture displays some features of an easy slip orientation {110} on the disc surface. At 1073 K the hardness reaches a plateau as shown in Fig. 5 and full recrystallization produces a strong and sharp {110} texture on the surface.

## 4. Discussion

### *4.1 Strength and ductility development during HPT processing and post-HPT annealing*

Through HPT processing of pure vanadium by up to 10 turns, the microstructure experiences significant grain refinement as shown in Fig. 1. Thus, the grain size is reduced

from an initial value of ~27 μm in the as-annealed state to a final value of ~410 nm with ~90% high-angle boundaries after processing through 10 turns. Accompanying the microstructural changes during HPT processing, it is apparent from Fig. 3 that the hardness increases from an initial value of Hv ≈ 85 to ~240 after 10 turns of HPT. This microstructural refinement and hardness improvement during HPT is consistent with the only other reports describing the HPT processing of vanadium [23, 24].

The tensile results in Fig. 6 show there is an increase from an initial value of ~260 to ~920 MPa after 10 turns but with a corresponding reduction in elongation from ~79% to ~29%. This strength and ductility paradox matches other reports for the HPT processing of an Al-1% Mg alloy [30] and pure tantalum [31] where it was shown that short-term annealing after HPT processing produced a small reduction in strength but a significant increase in ductility.

In the present experiments on vanadium, the effects of short-term annealing are summarized in Table 2. From inspection of these data and the microstructures in Fig. 4, it is apparent that short-term annealing at 773 K has very little effect and, conversely, short-term annealing at 1073 K produces very significant grain growth because of the onset of recrystallisation at 973 K. Thus, a retention of high strength combined with the occurrence of enhanced ductility requires short-term annealing at an intermediate temperature of ~873 K.

*4.2 The yield point phenomenon in the post-HPT annealed samples*

It is apparent from Fig. 6 that the vanadium samples subjected to post-HPT annealing at 873 and 973 K display a significant yield drop during room temperature testing at a strain rate of ~$10^{-3}$ $s^{-1}$. Generally, yield drops are associated with the presence of interstitial atoms such as carbon and nitrogen which are introduced as alloying elements so that dislocations are pinned to these interstitial solutes during plastic flow and hence become immobile. Thus, when a dislocation is pinned a small extra force is required to unpin the dislocation prior to

yielding and this produces an upper yield point in the stress-strain curve. After unpinning, the dislocations are free to move so that there is a lower yield point and the material deforms plastically.

Yielding point effects were reported in electro-refined vanadium containing 90 ppm carbon, 30 ppm nitrogen and 35 ppm oxygen when testing at room temperature with a strain rate of ~$10^{-3}$ $s^{-1}$ [3]. However, the vanadium used for the present experiments had a purity of 99.8% and no analysis is available showing the content of C, O and N. Nevertheless, it is known that vanadium oxidises in air at a temperature of about 660°C (933 K) and an oxide layer forms on the surface even at room temperature [32]. Considering the ultrafine-grained structure produced in vanadium after 10 turns of HPT, it is reasonable to anticipate that the multiplicity of boundaries will lead to enhanced diffusion. It is possible, therefore, that post-HPT annealing at 873 and 973 K leads to oxygen diffusion into the vanadium and this is the origin of the abrupt yield point that is especially present in post-HPT annealing at intermediate temperatures of the order of ~873 K.

In support of this conclusion, there are reports of unexpected yield point phenomena in ultrafine-grained materials such as commercial purity aluminium and ultra-low carbon interstitial free (IF) steel [33,34] and in a ferrite-cementite low carbon steel [35]. It was also reported earlier that when the grain size was increased above ~4 μm in commercial purity aluminium [34] and above ~2 μm in an ultra-low carbon steel [35] the materials showed smooth yielding behaviour.

*4.3 A comparison of properties after HPT, ECAP and ECAP with cryorolling*

The objective of this research was to achieve a high strength vanadium with improved ductility by using SPD processing through HPT. It is appropriate, therefore, to make a direct comparison with data available for the processing of vanadium using ECAP [11,21] and ECAP plus cryorolling [22]. These results are summarized in Table 3.

Using Tables 2 and 3 it is possible to directly compare vanadium processed by different procedures. However, in order to conduct a meaningful comparison, it is first necessary to note that the HPT and ECAP samples have different dimensions prior to the tensile testing. It was shown earlier, in a detailed examination of the effect of specimen dimensions on the tensile behaviour of ultrafine-grained Cu, that the measured elongations to failure tend to increase with decreasing gauge length [36]. This effect was later confirmed by finite element modelling and it was further suggested that the best criteria for examining tensile ductilities of samples having different initial dimensions is simply to compare the differing extents of the uniform elongations [37]. Unfortunately, this information is not generally available and therefore it is necessary to use an alternative approach. It is also worth noting that, although not directly relevant to the present research, a comparison of different specimen dimensions was also developed recently for tensile specimens prepared from thin films [38].

Table 2 shows that as-annealed vanadium, when cut to the dimensions of the HPT tensile samples but not processed by HPT, has a UTS of ~260 MPa and an elongation to failure of ~79%. By contrast, Table 3 shows that as-annealed vanadium has a UTS of ~247 MPa and an elongation of ~57% when tested with a gauge length of 13 mm and cross-sectional gauge dimensions of $3 \times 2$ mm$^2$ [21]. These results confirm that the UTS values are fairly similar in both sets of samples but the elongation is increased by a factor of ~38% in the miniature HPT samples due to the much reduced gauge length. Using this information as a guide, it is possible to directly compare the results obtained after processing by HPT, ECAP and ECAP plus cryorolling.

First, it is readily apparent that vanadium processed through 10 turns of HPT has a strength of ~920 MPa and an elongation of ~29% and this is superior to vanadium processed by ECAP for 8 passes where the UTS was ~751 MPa but the elongation was only ~15% [11].

Thus, the HPT sample is significantly stronger after processing and the ductility is improved by comparison with the ECAP sample even when the differing gauge lengths are taken into account. Second, there was an earlier attempt to increase the material strength using ECAP plus cryorolling and this combined procedure gave a UTS of ~918 MPa but with a much reduced elongation of ~8.5% [22]. This UTS essentially matches the value of ~920 MPa achieved after 10 turns of HPT but the elongation is very much lower than the value of ~29% in HPT and the difference cannot be fully attributed to the difference in gauge length. Furthermore, processing by HPT for 10 turns and annealing for 15 minutes at 873 K gave a UTS of ~750 MPa and an even more impressive elongation of ~39%.

All of these comparisons demonstrate that superior properties may be achieved most readily in vanadium by processing using HPT to produce a material that is both stronger and more ductile than may be achieved using other techniques. Furthermore, the present results show that the overall ductility may be increased with only a minor loss in strength by combining the HPT with a short post-HPT annealing treatment.

## 5. Summary and conclusions

1. Pure vanadium processed by HPT at room temperature achieved a significant grain refinement and strength enhancement. The grain size was reduced from an initial value of ~27 μm to ~400 nm and the hardness increased from Hv ≈ 85 to ~240 after 10 turns of HPT.

2. The microstructure was markedly inhomogeneous after 1/2 turn but gradually developed into a reasonably homogeneous structure with ~90% of high-angle grain boundaries after 10 turns of HPT processing.

3. Results from room temperature tensile testing show the HPT-processed vanadium has high strength with UTS ≈ 920 MPa and good ductility with ~29% elongation. The results demonstrate that, even when considering the reduced gauge lengths in HPT tensile specimens,

the HPT-processed vanadium has superior mechanical properties by comparison with vanadium processed by ECAP or ECAP plus cryorolling.

4. The introduction of a short-term (15 min) anneal at 873 K following the HPT is effective in providing improved ductility with an elongation of ~39% while at the same time retaining a high level of strength with a UTS of ~750 MPa.

**Acknowledgement**

This work was supported by the European Research Council under ERC Grant Agreement No. 267464-SPDMETALS.

**References**


[1] T.E. Tietz, J.W. Wilson, Behaviour and properties of refractory metals, Stanford University Press, Stanford, CA, 1965, p. 347.

[2] T.D. Joseph, M. Tanaka, A.J. Wilkinson, S.G. Roberts, Brittle-ductile transitions in vanadium and iron-chromium, J. Nuclear Mater. 367-370 (2007) 637-643.

[3] E.A. Loria, Some aspects of vanadium metallurgy in reference to nuclear reactor applications, J. Nuclear Mater. 61 (1976) 158-168.

[4] R.F. Mattas, B.A. Loomis, D.L. Smith, Vanadium alloys for fusion reactor applications, JOM 44 (8) (1992) 26-29.

[5] D.L. Smith, H.M. Chung, B.A. Loomis, H. Matsui, S. Votinov, W. Van Witzenburg, Development of vanadium-base alloys for fusion first-wall-blanket applications, Fusion Eng. Design 29 (1995) 399-410.

[6] H.M. Chung, B.A. Loomis, D.L. Smith, Development and testing of vanadium alloys for fusion applications, J. Nuclear Mater. 239 (1996) 139-156.

[7] Y. Wang, M. Kanedome, T. Yasuda, T. Suda, S. Watanabe, S. Ohnuki, T. Nagasaka, T. Muroga, Dynamic and static hydrogen effects on mechanical properties in pure vanadium, J. Nuclear Mater. 329-333 (2004) 477-480.

[8] H. Kurishita, T. Kuwabara, M. Hasegawa, Development of fine-grained V-28Cr-2.3Y and V-52Cr-1.8Y alloys with superior mechanical properties, Mater. Sci. Eng. A433 (2006) 32-38.

[9] N. Hasimoto, T.S. Byun, K. Farrell, S.J. Zinkle, Deformation microstructure of neutron-irradiated pure polycrystalline vanadium, J. Nuclear Mater. 336 (2005) 225-232.

[10] T. Kuwabara, H. Kurishita, M. Hasegawa, Development of an ultra-fine grained V-1.7 mass%Y alloy dispersed with yttrium compounds having superior ductility and high strength, Mater. Sci. Eng. A417 (2006) 16-23.

[11] Y.B. Chun, S.H. Ahn, D.H. Shin, S.K. Hwang, Grain refinement of vanadium by low temperature severe plastic deformation, Mater. Sci. Forum 638-642 (2010) 1934-1939.

[12] D. Xie, K. Liu, Y. Xian, L. Ye, Y. Chen, Effect of annealing temperature on the microstructure and properties of pure vanadium, Rare Metals Mater. Eng., 37 (2008) 1566-1569.

[13] R.Z. Valiev, R.K. Islamgaliev, I.V. Alexadrov, Bulk nanostructured materials from severe plastic deformation, Prog. Mater. Sci. 45 (2000) 103-189.

[14] T.G. Langdon, Twenty-five years of ultrafine-grained materials: Achieving exceptional properties through grain refinement, Acta Mater. 61 (2013) 7035-7059.

[15] Y. Huang, T.G. Langdon, Advances in ultrafine-grained materials, Mater. Today 16 (2013) 85-92.

[16] R.Z. Valiev, T.G. Langdon, Principles of equal-channel angular pressing as a processing tool for grain refinement, Prog. Mater. Sci. 51(2006) 881-981.

[17] A.P. Zhilyaev, T.G. Langdon, Using high-pressure torsion for metal processing: Fundamentals and applications, Prog. Mater. Sci. 53 (2008) 893-979.

[18] A.P. Zhilyaev, B.-K. Kim, G.V. Nurislamova, M.D. Baró, J.A. Szpunar, T.G. Langdon, Orientation imaging microscopy of ultrafine-grained nickel, Scripta Mater. 46 (2002) 575-580.

[19] A.P. Zhilyaev, G.V. Nurislamova, B.-K. Kim, M.D. Baró, J.A. Szpunar, T.G. Langdon, Experimental parameters influencing grain refinement and microstructural evolution during high-pressure torsion, Acta Mater. 51 (2003) 753-765.

[20] J. Wongsa-Ngam, M. Kawasaki, T.G. Langdon, A comparison of microstructures and mechanical properties in a Cu-Zr alloy processed using different SPD techniques, J. Mater. Sci. 48 (2013) 4653-4660.

[21] Z.Z. Jiang, S.H. Yu, Y.B. Chun, D.H. Shin, S.K. Hwang, Grain refinement of pure vanadium by equal channel angular pressing, Mater. Sci. Eng. A479 (2008) 285-292.

[22] Y.B. Chun, S.H. Ahn, D.H. Shin, S.K. Hwang, Combined effects of grain size and recrystallization on the tensile properties of cryorolled pure vanadium, Mater. Sci. Eng. A508 (2009) 253-258.

[23] S. Lee, K. Edalati, Z. Horita, Microstructure and mechanical properties of pure V and Mo processed by high-pressure torsion, Mater. Trans. 51 (2010) 1072-1079.

[24] A. Hohenwarter, S. Wurster, Deformation and fracture characteristics of ultrafine-grained vanadium, Mater. Sci. Eng. A650 (2016) 492-496.

[25] R.B. Figueiredo, P.R. Cetlin, T.G. Langdon, Using finite element modeling to examine the flow processes in quasi-constrained high-pressure torsion, Mater. Sci. Eng. A528 (2011) 8198-8204.

[26] R.B. Figueiredo, P.H.R. Pereira, M.T.P. Aguilar, P.R. Cetlin, T.G. Langdon, Using finite element modeling to examine the temperature distribution in quasi-constrained high-pressure torsion, Acta Mater. 60 (2012) 3190-3198.

[27] M. Kawasaki, T.G. Langdon, The significance of strain reversals during processing by high-pressure torsion, Mater. Sci. Eng. A498 (2008) 341-348.

[28] A. Loucif, R.B. Figueiredo, M. Kawasaki, T. Baudin, F. Brisset, R. Chemam, T.G. Langdon, Effect of aging on microstructural development in an Al–Mg–Si alloy processed by high-pressure torsion, J. Mater. Sci. 47 (2012) 7815-7820.

[29] L.S. Tóth, B. Beausir, C.F. Gu, Y. Estrin, N. Scheerbaum, C.H.J. Davies, Effect of grain refinement by severe plastic deformation on the next-neighbor misorientation distribution, Acta Mater. 58 (2010) 6706-6716.

[30] O. Andreau, J. Gubicza, N.X. Zhang, Y. Huang, P. Jenei, T.G. Langdon, Effect of short-term annealing on the microstructures and flow properties of an Al–1% Mg alloy processed by high-pressure torsion, Mater. Sci. Eng. A615 (2014) 231-239.

[31] N. Maury, N.X. Zhang, Y. Huang, A.P. Zhilyaev, T.G. Langdon, A critical examination of pure tantalum processed by high-pressure torsion, Mater. Sci. Eng. A638 (2015) 174-182.

[32] A.D. Hammond, Vanadium, the green metal: Mineral deposits in the Colorado Plateau, Mining Eng., 65 (12) (2013) 1-8.

[33] N. Tsuji, Y. Ito, Y. Saito, Y. Minamino, Strength and ductility of ultrafine grained aluminium and iron produced by ARB and annealing, Scripta Mater. 47 (2002) 893-899.

[34] C.Y. Yu, P.W. Kao, C.P. Chang, Transition of tensile deformation behaviours in ultrafine-grained aluminium, Acta Mater. 53 (2005) 4019-4028.

[35] N. Tsuchida, H. Masuda, Y. Harada, K. Fukaura, Y. Tomota, K. Nagai, Effect of ferrite grain size on tensile deformation behavior of a ferrite-cementite low carbon steel, Mater. Sci. Eng. A488 (2008) 446-452.

[36] Y.H. Zhao, Y.Z. Guo, Q. Wei, A.M. Dangelewicz, C. Xu, Y.T. Zhu, T.G. Langdon, Y.Z. Zhou, E.J. Lavernia, Influence of specimen dimensions on the tensile behavior of ultrafine-grained Cu, Scripta Mater. 59 (2008) 627-630.

[37] Y.H. Zhao, Y.Z. Guo, Q. Wei, T.D. Topping, A.M. Dangelewicz, Y.T. Zhu, T.G. Langdon, E.J. Lavernia, Influence of specimen dimensions and strain measurement methods on tensile stress–strain curves, Mater. Sci. Eng. A525 (2009) 68-77.

[38] J.A. Sharon, H.A. Padilla, B.L. Boyce, Interpreting the ductility of nanocrystalline metals, J. Mater. Res. 28 (2013) 1539-1552.

**Figure captions**

Fig. 1 Microstructures after HPT processing: (a), (c), (e) and (g) show the centre areas after 1/2, 1, 5 and 10 turns, (b), (d), (f) and (h) show the edge areas after 1/2, 1, 5 and 10 turns.

Fig. 2 Distributions of grain boundary misorientations after HPT processing at (a) centre area and (b) edge area.

Fig. 3 Colour-coded maps of the Vickers microhardness values after HPT processing through 1/2, 1, 5 and 10 turns: the colour key is shown at the lower right.

Fig. 4 Microstructures after post-HPT annealing at (a) 773 K, (b) 873 K, (c) 973 K and (d) 1073 K.

Fig. 5 Variation of microhardness and grain size with post-HPT annealing temperature.

Fig. 6 Stress-strain curves at a strain rate of $1.5 \times 10^{-3}$ $s^{-1}$ for the as-annealed material, 10 turns HPT sample and 10 turns HPT samples with subsequent post-HPT annealing at 773, 873 or 973 K.

Fig. 7 Inverse pole figures in normal direction to HPT disc surface for samples after HPT processing at the centre and edge after 1/2 turn (upper row) and after 10 turns (lower row).

Fig. 8 Inverse pole figures in normal direction to HPT disc surface for samples after post-HPT short-term annealing at 873, 973 and 1073 K

**Table captions**

Table 1 Fractions of low-angle grain boundaries (LAGBs) and high-angle grain boundaries (HAGBs) in disc centres and edges after different numbers of HPT turns.

Table 2 Tensile results for vanadium.

Table 3 Tensile results for vanadium from other investigations.

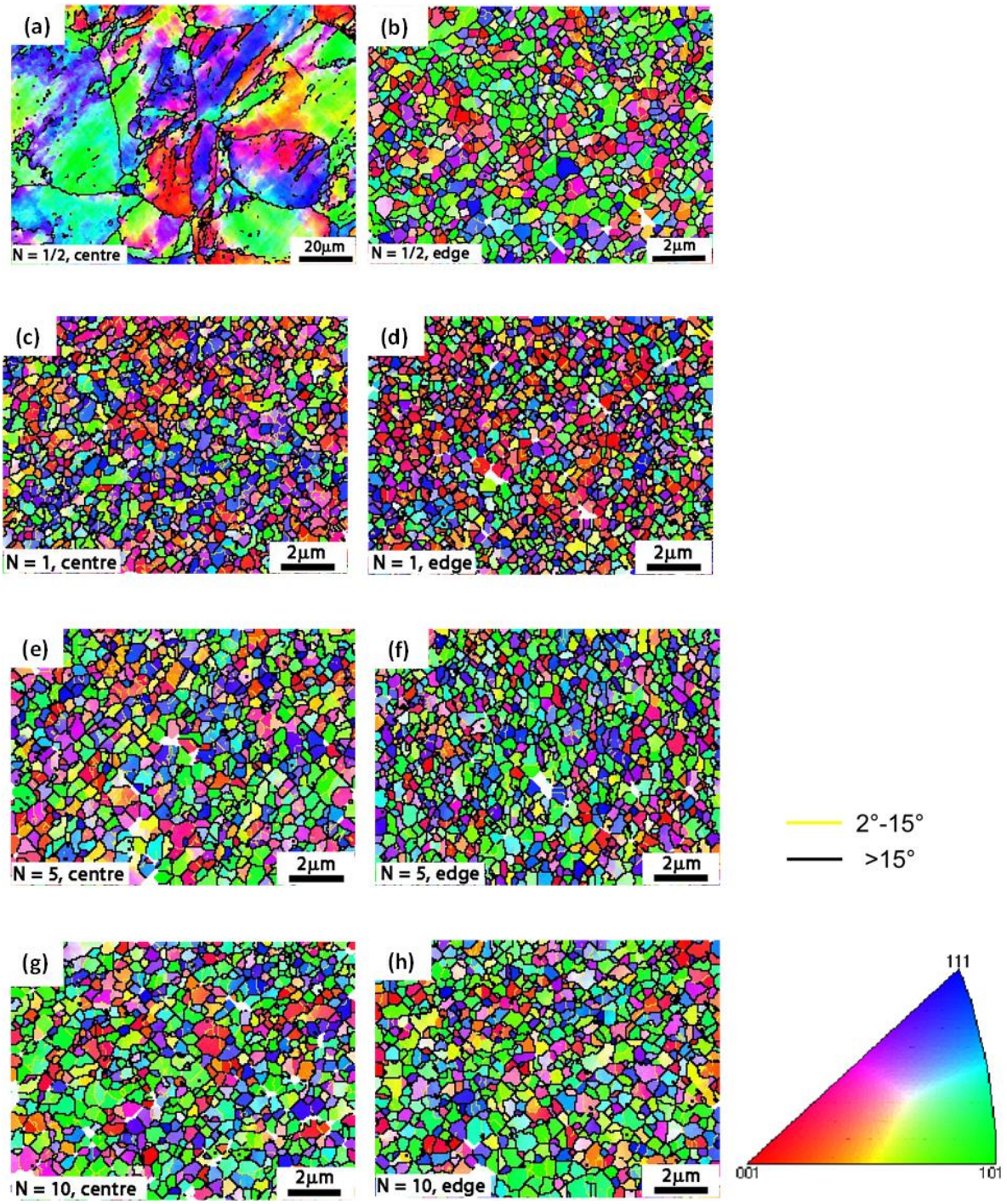


Fig. 1 Microstructures after HPT processing: (a), (c), (e) and (g) show the centre areas after 1/2, 1, 5 and 10 turns, (b), (d), (f) and (h) show the edge areas after 1/2, 1, 5 and 10 turns.

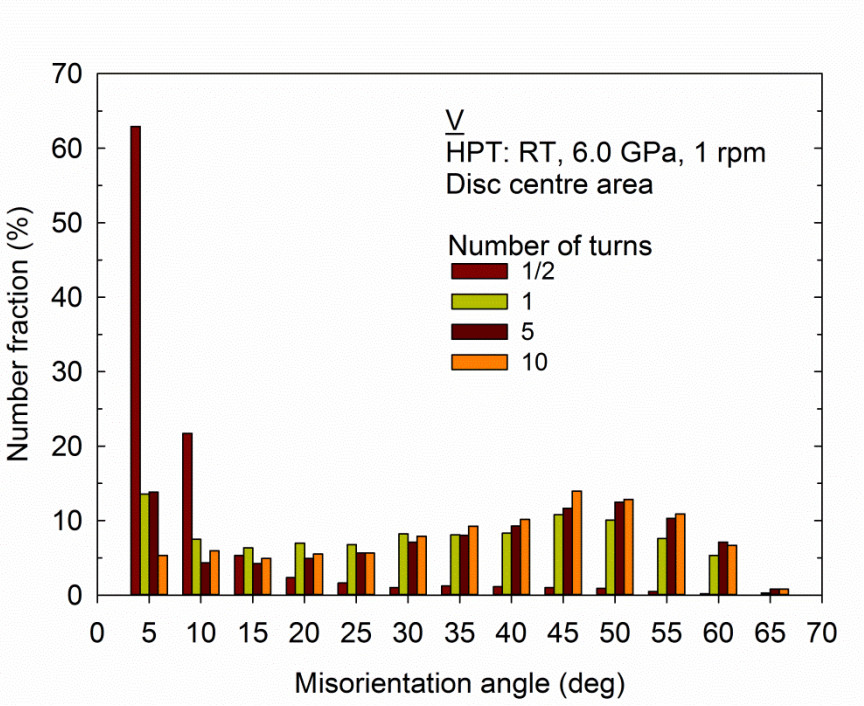


(a)

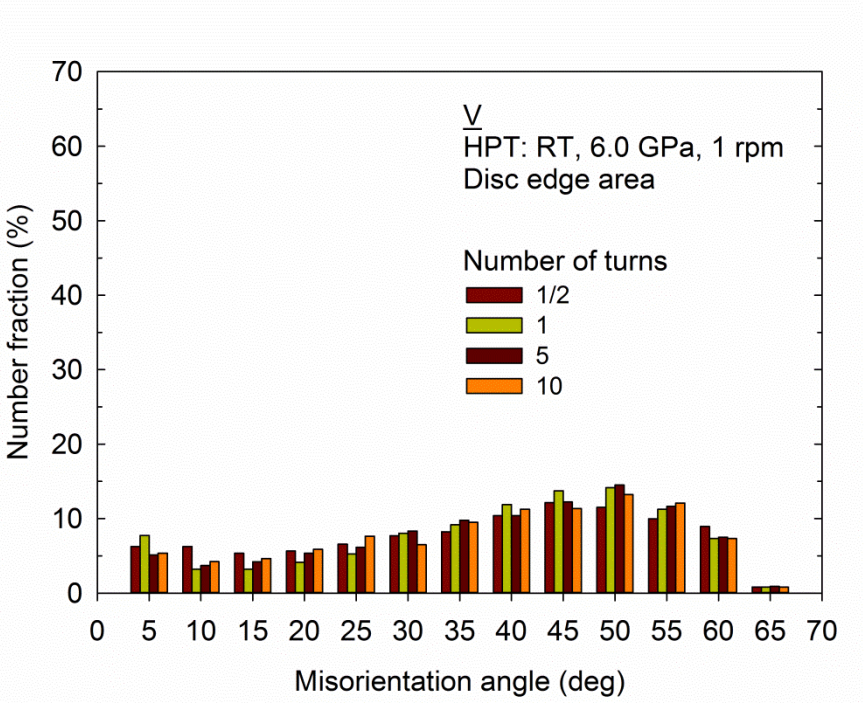


(b)

Fig. 2 Distributions of grain boundary misorientations after HPT processing at (a) centre area and (b) edge area.

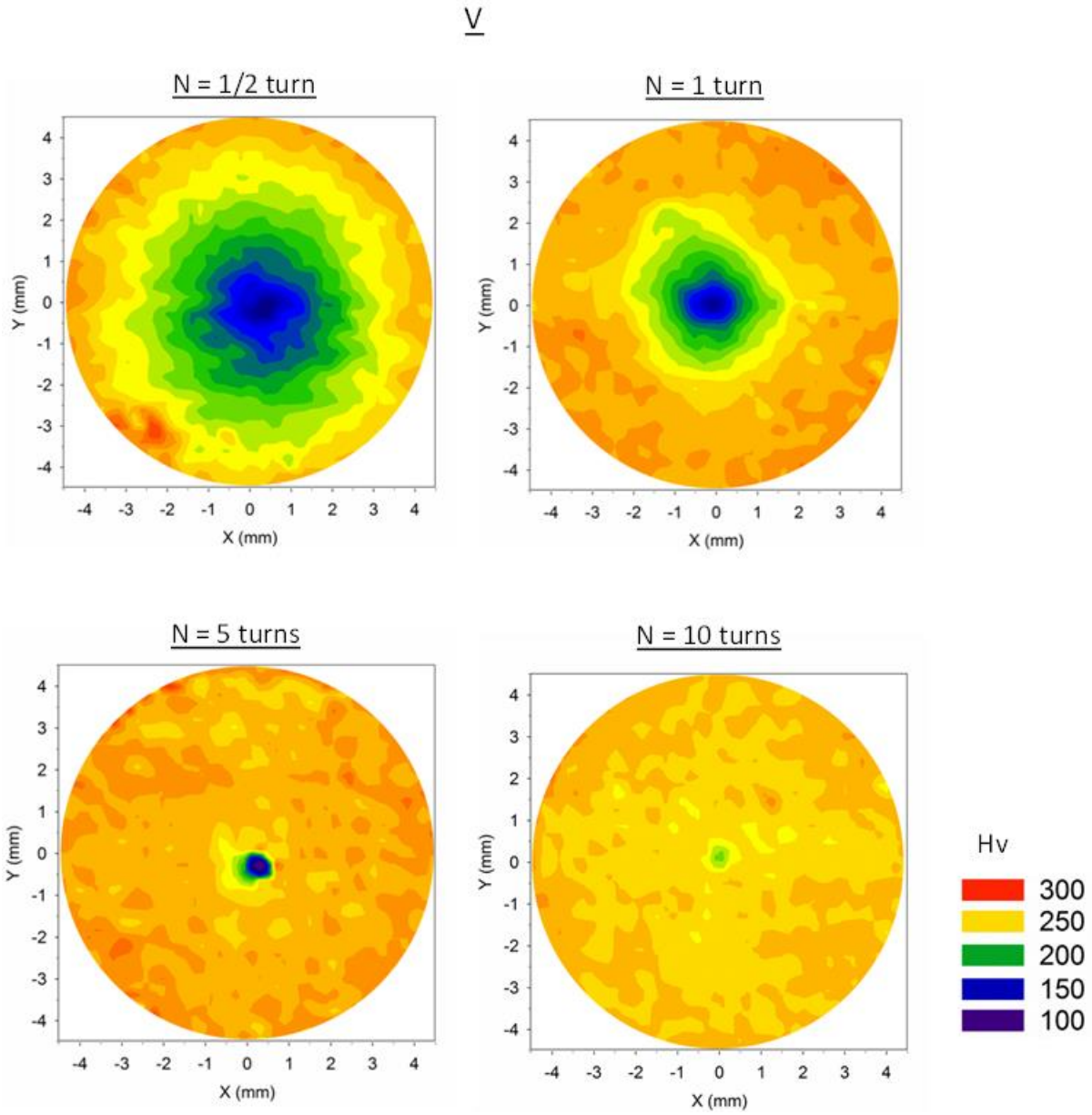


Fig. 3 Colour-coded maps of the Vickers microhardness values after HPT processing through 1/2, 1, 5 and 10 turns: the colour key is shown on the lower right.

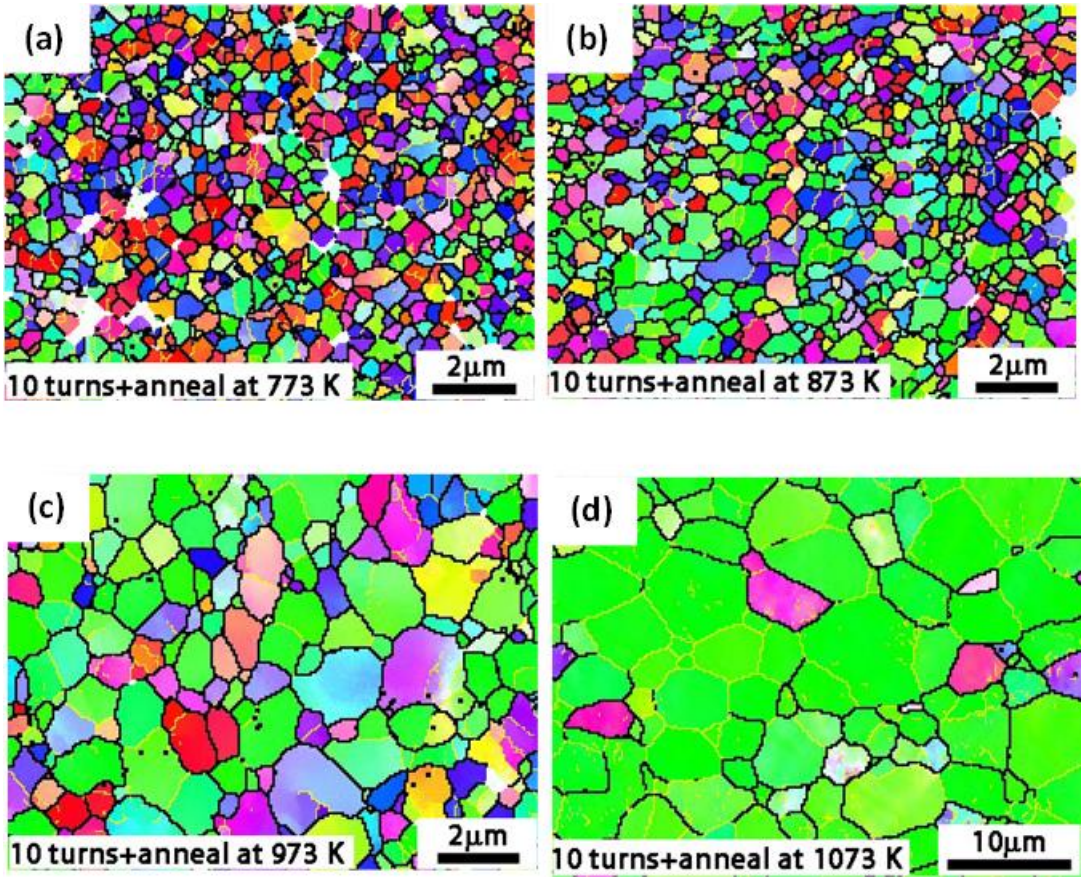


Fig. 4 Microstructures after post-HPT annealing at (a) 773 K, (b) 873 K, (c) 973 K and (d) 1073 K.

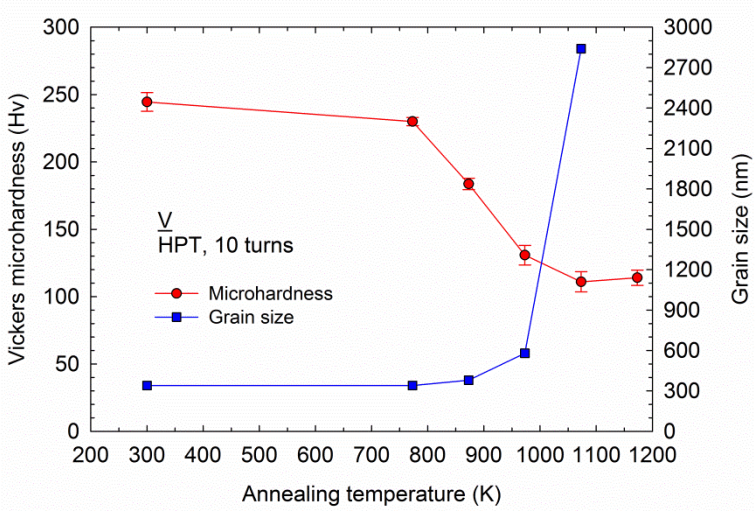


Fig. 5 Variation of microhardness and grain size with post-HPT annealing temperature.

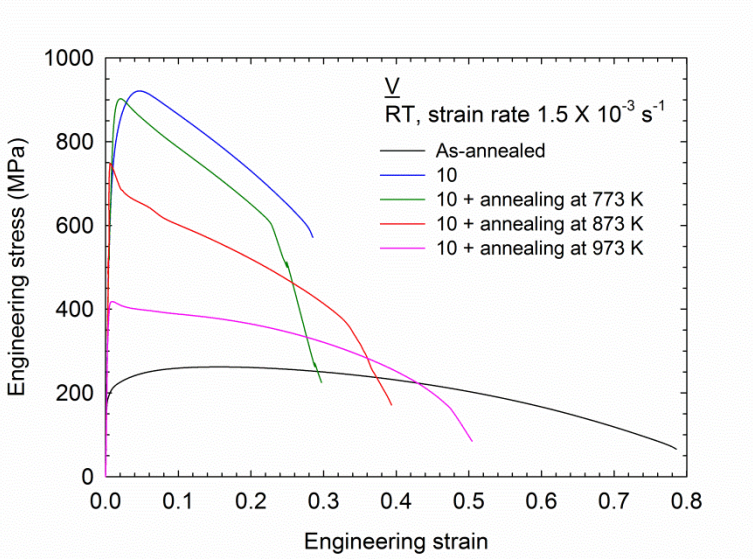


Fig. 6 Stress-strain curves at a strain rate of $1.5 \times 10^{-3}$ $s^{-1}$ for the as-annealed material, 10 turns HPT sample and 10 turns HPT samples with subsequent post-HPT annealing at 773, 873 and 973 K.

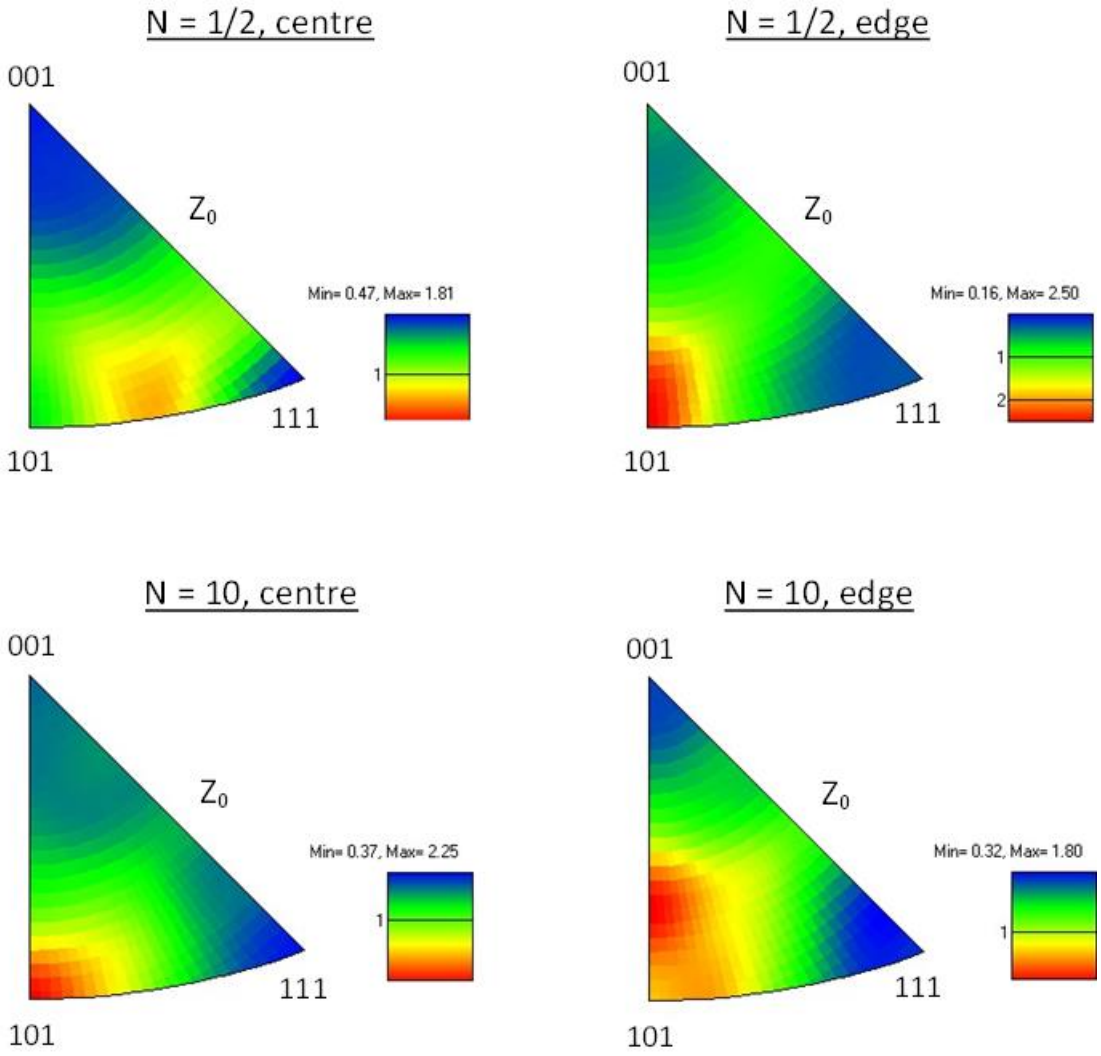


Fig. 7 Inverse pole figures in normal direction to HPT disc surface for samples after HPT processing at the centre and edge after 1/2 turn (upper row) and after 10 turns (lower row).

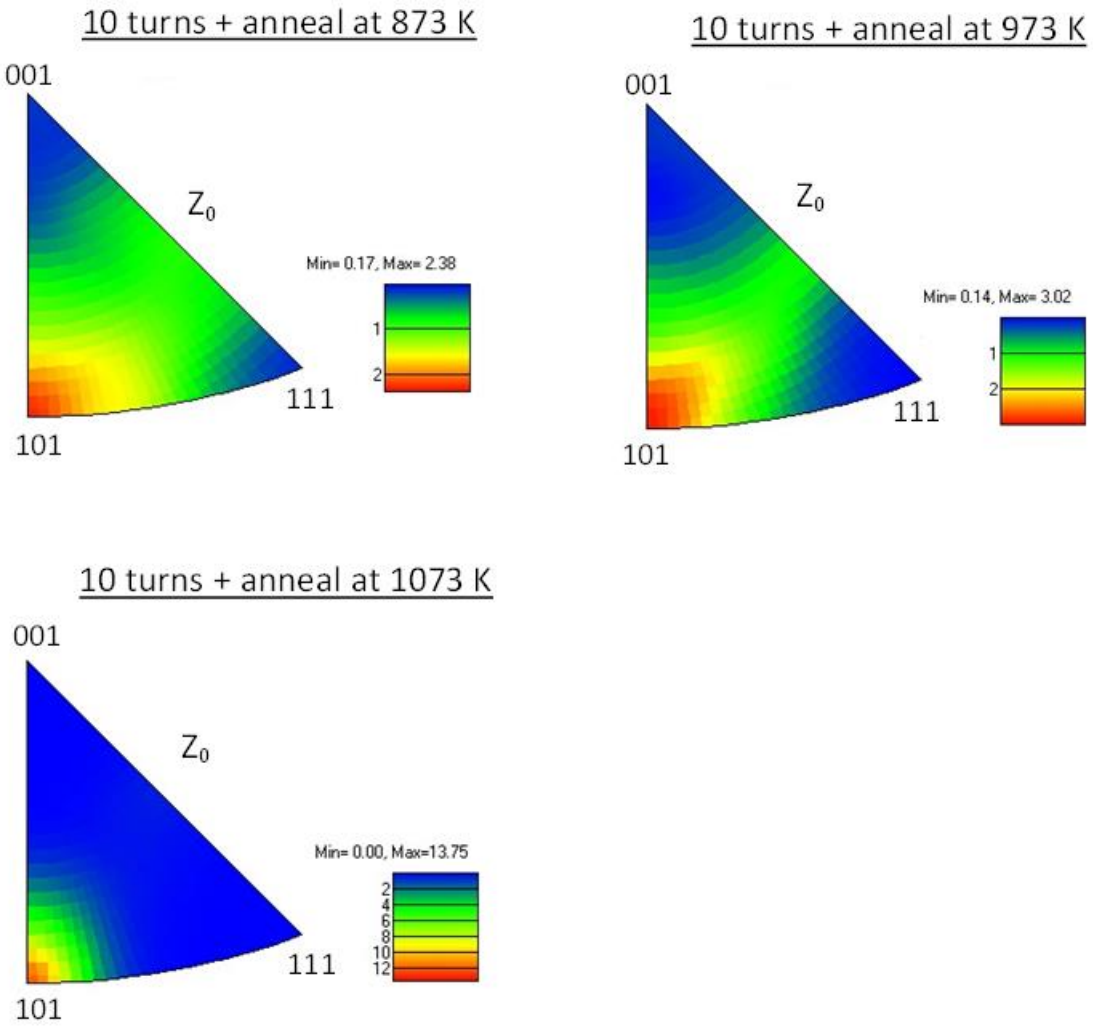


Fig. 8 Inverse pole figures in normal direction to HPT disc surface for samples after post-HPT annealing at 873, 973 and 1073 K.